

Testing for Features in the Primordial Power Spectrum

Loison Hoi and James M. Cline

Department of Physics, McGill University

3600 Rue University, Montréal, Québec, Canada H3A 2T8

E-mail: hoiloison@physics.mcgill.ca, jcline@physics.mcgill.ca

December 22, 2009

Abstract

Well-known causality arguments show that events occurring during or at the end of inflation, associated with reheating or preheating, could contribute a blue component to the spectrum of primordial curvature perturbations, with the dependence k^3 . We explore the possibility that they could be observably large in CMB, LSS, and Lyman- α data. We find that a k^3 component with a cutoff at some maximum k can modestly improve the fits ($\Delta\chi^2 = 2.0, 5.4$) of the low multipoles ($\ell \sim 10 - 50$) or the second peak ($\ell \sim 540$) of the CMB angular spectrum when the three-year WMAP data are used. Moreover, the results from WMAP are consistent with the CBI, ACBAR, 2dFGRS, and SDSS data when they are included in the analysis. Including the SDSS galaxy clustering power spectrum, we find weak positive evidence for the k^3 component at the level of $\Delta\chi^{2'} = 2.4$, with the caveat that the nonlinear evolution of the power spectrum may not be properly treated in the presence of the k^3 distortion. To investigate the high- k regime, we use the Lyman- α forest data (LUQAS, Croft *et al.*, and SDSS Lyman- α); here we find evidence at the level $\Delta\chi^{2'} = 3.8$. Considering that there are two additional free parameters in the model, the above results do not give a strong evidence for features; however, they show that surprisingly large bumps are not ruled out. We give constraints on the ratio between the k^3 component and the nearly scale-invariant component, $r_3 < 1.5$, over the range of wave numbers $2.3 \times 10^{-3} \text{ Mpc}^{-1} < k < 8.2 \text{ Mpc}^{-1}$. We also discuss theoretical models which could lead to the k^3 effect, including ordinary hybrid inflation and double D-term inflation models. We show that the well-motivated k^3 component is also a good representative of the generic spikelike feature in the primordial perturbation power spectrum.

1 Introduction

Inflation has become a cornerstone of modern cosmology; it not only solves critical cosmological problems, but also provides possibilities of exploring the infant universe [1, 2, 3]. A crucial aspect of inflationary theory is the primordial perturbation power spectrum, which

connects the quantum fluctuations in the early universe to the formation of structure at later times. Inflation generically predicts a nearly scale-invariant primordial power spectrum, which agrees well with cosmic microwave background (CMB), large-scale structure (LSS), and Lyman- α forest observations, such as the Wilkinson Microwave Anisotropy Probe (WMAP) [4, 5], Cosmic Background Imager (CBI) [6], Arcminute Cosmology Bolometer Array Receiver (ACBAR) [7], Two-degree-Field Galaxy Redshift Survey (2dFGRS) [8, 9], Sloan Digital Sky Survey (SDSS) [10, 11], and Lyman- α forest (Viel *et al.* [12, 13, 14] and SDSS Lyman- α [15, 16]).

While producing a nearly scale-invariant spectral index has become a major criterion of model selection, a deviation from pure scale invariance is consistent with the current data, and in fact fits better than $n_s = 1$. Further elaborations have been investigated; a well-known example, suggested by the first-year WMAP data (WMAP1) [17], is the running spectral index model, which has a large and negative running of the spectral index and a large tensor-to-scalar ratio (although the evidence for this is weakened when the three-year WMAP data [WMAP3] is used [5]). Detailed investigation revealed that a partially running spectral index model, which has a constant spectral index on large and small scales but a running spectral index on the relevant scales (about 3.4 e-foldings), provides as good a fit to WMAP1 as the full running spectral index model [18]. Because of the limited range of scales, this could be described as adding a localized *feature* to the primordial spectrum, a topic which has also received considerable attention [19, 20, 21, 22], and which is the theme of the present work.

Other hints of peculiarities in the CMB data have prompted the investigation of spectral features going beyond a simple power law. For example, the reconstruction of the primordial power spectrum directly from the CMB angular spectrum data indicates the prominent feature of an infrared cutoff on the horizon scale [23, 24]. There are also a few outlying multipoles at smaller scales, $\ell \sim 10 - 50$ and $\ell \sim 540$, which have inspired modifications to the spectrum, such as would be provided by introducing a sharp step in the inflaton potential [17, 19, 20, 21]. This introduces oscillations into the spectrum which allow for better fits to the data [25, 26]. More recent analyses of this subject can be found in Refs. [27, 28, 29, 30, 31, 32, 33, 34, 35, 36, 37, 38]. Such improvements of course come at the price of adding more parameters to the model; questions of significance can be handled through quantitative model selection criteria [39, 40, 41, 42].

Because the current data do not justify adding a large number of parameters to the description of the power spectrum, it is important to consider models with a small number of extra parameters, and preferably with a strong theoretical motivation. In the present work, we will investigate a new kind of spectral feature in this category, namely the addition of a component which scales like k^3 , in contrast to the nearly scale-invariant spectrum $\sim k^0$. As we will describe in Section 2, this behavior was a generic prediction [43] based on the requirement of causality, prior to the invention of inflation. Our observation is that extra contributions to the spectrum arising after inflation, for example during reheating, could be expected to scale like k^3 at low k . In fact, it was recently shown that this effect can arise in hybrid inflation models [44, 45] and double D-term inflation models [46].

Of course, other qualitatively similar distortions could arise in particular inflationary models, having k^n spectra with $n \neq 3$. In this paper we focus on the $n = 3$ case because of the theoretical motivations mentioned above, and upon which we will elaborate further

below. However, for much of our analysis of the data, we would not expect greatly different results for nearby values like $n = 2$ or $n = 4$, for the reason that the large- k behavior must be cutoff at some scale k_c ; then the feature of interest is a localized spike (since the data do not allow for larger features) which would exceed the underlying scale-invariant contribution to $\mathcal{P}_{\mathcal{R}}(k)$ only over a rather limited range of k . In that sense, the k^3 model with a cutoff can be considered as a rather generic model for spikelike features in the primordial power spectrum. Nevertheless, we will compare the k^3 spike to k^n spikes with $n = 1, 2, 4, 5$, which will clarify this point. Spikelike features in the primordial power spectrum have been previously investigated in the literature. For example, Ref. [22] finds a strong spike in the smooth hybrid inflation model; its location, however, is beyond the current CMB-LSS scales and hence is not observable. In any case, we take the point of view that the k^3 model (with a cutoff) is sufficiently well-motivated to provide an interesting test for a feature of this kind, and we have done a state-of-the-art comparison of this model of spectral features with the CMB, LSS, and Lyman- α data.

To describe the k^3 effect, we modify the primordial curvature power spectrum, $\mathcal{P}_{\mathcal{R}}(k) \equiv (L/2\pi)^3 4\pi k^3 \langle |\mathcal{R}_{\mathbf{k}}|^2 \rangle$ (see Appendix A), to the form

$$\begin{aligned} \mathcal{P}_{\mathcal{R}}(k) &= \mathcal{P}_{\phi}(k) + \mathcal{P}_3(k) \\ &= \mathcal{P}_{\phi}(k_0) \left(\frac{k}{k_0}\right)^{n_s-1} + \mathcal{P}_3(k_0) \left(\frac{k}{k_0}\right)^3 \\ &= \mathcal{P}_{\phi}(k_0) \left[\left(\frac{k}{k_0}\right)^{n_s-1} + r_3(k_0) \left(\frac{k}{k_0}\right)^3 \right], \end{aligned} \quad (1)$$

where k_0 is a pivot point which we take to be $k_0 = 0.002 \text{ Mpc}^{-1}$ throughout (to be consistent with the WMAP collaboration). The amplitude ratio of the k^3 component to the nearly scale-invariant component is

$$r_3(k) \equiv \frac{\mathcal{P}_3(k)}{\mathcal{P}_{\phi}(k)}. \quad (2)$$

We refer to the model whose power spectrum is described by Eq. (1) as the k^3 model. It has just one free parameter relative to the power-law Λ CDM model: the ratio r_3 . However, in any realistic model, the k^3 behavior must be cut off at some maximum scale k_c ; for example, in tachyonic preheating, where the tachyon curvature m_{σ}^2 is negative, only the perturbations satisfying $k^2 < a^2|m_{\sigma}^2|$ are amplified. For simplicity we introduce a sharp cutoff: if $k > k_c$, then the k^3 term in Eq. (1) is set to 0. We refer to this as the k_c^3 model. It has one more parameter, k_c .

In this paper, we examine the extent to which the k_c^3 model is consistent with the data. We begin in Section 2 by reviewing the theoretical motivations for this effect. Section 3 continues with a brief description of the CMB, LSS, and Lyman- α data used in the analysis. We investigate the evidence from WMAP in Section 4, and explore the k^3 component on small scales by the high- ℓ CMB, LSS, and Lyman- α data in Section 5. In Section 6 we explore the parameter space of hybrid inflation and double D-term inflation models which could give parameters suggested by the previous phenomenological analysis. We compare the k^3 spike to more general k^n spikes in Section 7. We give conclusions in Section 8. In

Appendix A we clarify the relation between the k^3 spectrum (in modern notation) and the causality prediction made in the early literature.

2 Motivation for the k^3 component

Prior to the idea of inflation, it was argued on the basis of causality that any fluctuations which are created independently of each other must have a correlation function that vanishes at least as fast as k^3 as $k \rightarrow 0$. This was first proven in the context of Newtonian gravity and then extended to general relativity in Ref. [43]. In Appendix A we recapitulate (and translate into modern notation) this argument. The essential observation is that a density perturbation $\delta\rho(\mathbf{x})/\rho$ which consists of contributions from causal processes originating at positions \mathbf{x}_a has the form

$$\frac{\delta\rho(\mathbf{x})}{\rho} = \sum_a F_a(\mathbf{x} - \mathbf{x}_a), \quad (3)$$

where causality demands that the monopole and dipole moments of F_a vanish in a volume extending over distances greater than the causal horizon [47, 48]. In Fourier space, this implies that $F_{a\mathbf{k}}$ must vanish at least as fast as k^2 for small k . Therefore the correlation $\langle |\delta\rho_{\mathbf{k}}/\rho|^2 \rangle$ falls like k^4 at small k . Appendix A shows how this corresponds to a k^3 spectrum for the curvature perturbation.

Inflationary perturbations evade this constraint by having been in causal contact with each other before being driven out of causal contact by inflation. But perturbations produced at the end of inflation, or between two consecutive stages of inflation, for example during a phase of tachyonic preheating, should obey the constraint. A k^3 component could lead to interesting effects at short scales, such as the production of primordial black holes. It could conceivably also distort the spectrum of CMB fluctuations at longer scales, if it is appropriately cut off at the short scales. Of course, there is no reason to believe that the k^3 growth should continue to arbitrarily large k , since it is derived in the region $k \rightarrow 0$, and unrestricted growth at large k would lead to an unphysical UV divergence in the power. The value of the cutoff k_c beyond which the effect vanishes depends on the particular model giving rise to it. In the case of tachyonic preheating, the cutoff is determined by the mass parameter (m_σ^2) of the tachyonic field, since only modes with physical wave number $k^2 < a^2|m_\sigma^2|$ at the time of preheating undergo exponential growth.

Explicit examples of k^3 spectral components have been discussed in Refs. [49, 50, 51]; they were generated by preheating at the end of chaotic inflation. It was shown that those models do not have enough freedom to give an observably large k^3 component once the COBE normalization is imposed. On the other hand, hybrid inflation models have more free parameters and thus have more likelihood to produce an observably large effect. In Ref. [46] it was noted that double (D-term) hybrid inflation models [52, 53, 54] can produce a spike with a k^3 spectrum and a cutoff, due to a tachyonic instability which triggers the transition between the two stages of inflation. More recently it has been shown [44, 45] that tachyonic preheating even in the simplest model of hybrid inflation can generate an observably large k^3 component or alternatively large non-Gaussianity (see also Refs. [55, 56, 57, 58]) for certain ranges of parameters. This effect arises at second order in the cosmological perturbation,

and its importance is controlled by how large the fluctuations of the tachyon field can become before their back-reaction ends inflation.

In Section 6 we will make a detailed study of the predictions of tachyonic preheating in the hybrid inflation for the k^3 perturbation and how it compares to the CMB and LSS data. In the next section we describe these data.

3 Data

To explore the experimental evidence for the k^3 component, we use CosmoMC, a publicly available Markov-chain Monte-Carlo (MCMC) engine for exploring cosmological parameter space [59].¹ We use the first year and three-year WMAP data (WMAP1 and WMAP3) [4, 5] as primary data sets, analyzing them with the July 2005 and May 2006 versions of CosmoMC, respectively. For completeness and as a consistency check, we consider both WMAP1 and WMAP3 in this work.

We include the high- ℓ CMB data, CBI [6] and ACBAR [7], to explore the evidence for the k^3 component on small scales. The ranges of data we use are $300 < \ell < 3500$ (14 data points) for CBI and $300 < \ell < 3000$ (13 data points) for ACBAR.² The first bands of both data are not included in the analysis since they are not well constrained.

The LSS data, 2dFGRS [8, 9] and SDSS main galaxy sample [10],³ are also used in our analysis. To use the linear theory, we set $k_{\max} = 0.15h \text{ Mpc}^{-1}$ in the galaxy-galaxy power spectrum as recommended by 2dFGRS and SDSS; their ranges are $0.022 \text{ Mpc}^{-1} < k/h < 0.147 \text{ Mpc}^{-1}$ for 2dFGRS (32 data points) and $0.016 \text{ Mpc}^{-1} < k/h < 0.154 \text{ Mpc}^{-1}$ for SDSS (17 data points). SDSS also probes the nonlinear regime, which allows us to explore the possibility of fitting the nonlinear regime with the k^3 component. The ranges are extended to $k/h = 0.205 \text{ Mpc}^{-1}$ (2 more data points). Further discussions can be found in Section 5.2. We also include the SDSS Luminous Red Galaxies (LRG) power spectrum [11]; the range is $0.012 \text{ Mpc}^{-1} < k/h < 0.087 \text{ Mpc}^{-1}$ (14 data points) for linear theory, and it is extended to $k/h = 0.203 \text{ Mpc}^{-1}$ (6 more data points) for nonlinear theory. The results of 2003 [10] and 2006 SDSS [11] data are referred to as SDSS1 and SDSS4, respectively, since they used the SDSS data release 1 and 4, respectively.

Lyman- α forest data allow us to explore the high- k regime. We use two different Lyman- α data sets to test the k^3 component. Viel *et al.* [12] used the LUQAS sample [13], which has $z = 2.125$, and its range is $0.0034 \text{ (km/s)}^{-1} < k < 0.027 \text{ (km/s)}^{-1}$; they also reanalyzed the result of Croft *et al.* [14] ($z = 2.72$) in the same range. The SDSS Lyman- α data [15, 16] have $2 < z < 4$ and the range is $0.0013 \text{ (km/s)}^{-1} < k < 0.02 \text{ (km/s)}^{-1}$.⁴ The data sets we

¹See <http://www.cosmologist.info/cosmomc>.

²The offset lognormal matrix for 2000 + 2001 CBI was incorrectly incorporated into May 2006 or earlier versions of CosmoMC [60], so we use our offset lognormal matrix in this paper. See Ref. [60] for a discussion on the impact of using the wrong matrix; also see the CBI website, <http://www.astro.caltech.edu/~tjp/CBI/data2004>, for a link to the discussion on this issue.

³2002 and 2005 2dFGRS data are used along with WMAP1 and WMAP3, respectively; the differences of the results, however, are not significant.

⁴For the SDSS Lyman- α data, we do not use the default code in CosmoMC; instead, we use the patch

use, from CMB, LSS, to Lyman- α forest, cover k space from 10^{-4} Mpc $^{-1}$ to 3 Mpc $^{-1}$ and provide full sensitivity to a possible k^3 component on observable scales.

In our comparison of the power-law Λ CDM model with the k^3 and k_c^3 models, we do not include the BB polarization power spectrum or the Sunyaev-Zel'dovich (SZ) effect. Most settings in CosmoMC are by default. Typical MCMC chains have on the order of 10^5 points and we search these chains to find the best fit points.

4 Evidence from WMAP: Large Scales

In this section we focus on the large scale (small k) region of the spectrum, using primarily the WMAP data to fit the k_c^3 model; for comparison we will also show the effect of combining with other CMB (CBI and ACBAR), LSS (2dFGRS or SDSS), or Lyman- α data. To get a significant effect at low k , the cutoff k_c is necessary in order to avoid being dominated by the large amount of extra power at high k . Table 1 lists the best fit k_c^3 models for WMAP alone, and in combination with other CMB (CBI and ACBAR), LSS (2dFGRS or SDSS), or Lyman- α data.

As can be seen in Table 1, the k_c^3 model improves the fit to the data, relative to that of the power-law Λ CDM model, by a reduction in the χ^2 of $\Delta\chi^2 = 3.6$ for the first year WMAP data, where

$$\Delta\chi^2 = \chi^2(\Lambda\text{CDM}) - \chi^2(k_c^3). \quad (4)$$

Recall that $\Delta\chi^2 = 4.7$ for the running spectral index + tensor model [61], and so the k_c^3 model is not as good as the running spectral index + tensor model when the first year WMAP data are used (both models have eight parameters). Nevertheless, the k_c^3 model gives a large amplitude ratio ($r_3(k_c) = 0.69$), and hence WMAP1 allows for a relatively large extra component in addition to the nearly scale-invariant spectrum, as shown in the top-left panel of Fig. 1. More intriguingly, for the three-year WMAP data, we find an improvement of $\Delta\chi^2 = 5.4$; recall that $\Delta\chi^2 = 3.1$ for the running spectral index + tensor model [61], and so the k_c^3 model gives a better fit than the running spectral index + tensor model using WMAP3. The top-right panel of Fig. 1 shows the spectra; it is interesting that a small modification ($r_3(k_c) = 0.14$) to the nearly scale-invariant spectrum can give such a large $\Delta\chi^2$.

To better understand why the k^3 term improves the fits, the C_ℓ^{TT} spectra are plotted. The lower part of Fig. 1 shows the best fit C_ℓ^{TT} spectra for the power-law Λ CDM model (solid, black) and the k_c^3 model (dashed, red) using the WMAP1 (left) and WMAP3 (right) data (dotted, green); the C_ℓ^{TE} spectra are hardly changed, so they are not shown. It can be seen that both spectra are consistent over a large range, but the C_ℓ^{TT} spectrum of the k_c^3 model provides a better fit at low multipoles ($\ell \sim 10 - 50$) when WMAP1 is used. Therefore, the k_c^3 model can help explain the ‘‘glitch’’ in the low multipoles of the C_ℓ^{TT} spectrum. It has also been argued that an exponentially increasing step [23, 24] or oscillations [25, 26] in the primordial power spectrum fit the low C_ℓ^{TT} multipoles better than the nearly scale-invariant spectrum. Since the peak of the k_c^3 model is similar to an exponentially increasing step or

provided by Anže Slosar. See <http://www.slosar.com/aslosar/lya.html>.

Table 1: Best fit k_c^3 models of fitting WMAP alone, and in combination with other CMB (CBI and ACBAR), LSS (2dFGRS or SDSS), or Lyman- α data. $\chi^{2'}$ is the contribution to χ^2 from all data excluding WMAP.

Data	$\chi^2/\chi^{2'}$ (Λ CDM)	$\Delta\chi^2/\Delta\chi^{2'}$ (k_c^3)	n_s (k_0)	$r_3(k_0)$	k_c (Mpc^{-1})	r_3 (k_c)
WMAP1	1428.8/-	3.6/-	1.005	0.0911	0.00394	0.694
+ CMB	1463.1/30.9	3.2/-2.5	0.987	0.0782	0.00385	0.561
+ 2dFGRS	1463.2/34.4	1.7/0.0	1.010	0.0280	0.00408	0.236
+ SDSS1 (linear)	1445.9/16.9	0.5/-0.2	0.987	0.0715	0.00356	0.407
+ SDSS4 (linear)	1443.3/12.5	3.8/-0.4	0.983	0.0123	0.00364	0.747
WMAP3	11252.3/-	5.4/-	0.944	1.62×10^{-5}	0.0388	0.139
+ CMB	11285.9/33.3	4.1/0.4	0.949	2.38×10^{-5}	0.0373	0.178
+ 2dFGRS	11290.8/38.4	3.7/-0.2	0.947	1.08×10^{-5}	0.0383	0.0890
+ SDSS1 (linear)	11274.0/18.9	4.5/-0.1	0.952	1.26×10^{-5}	0.0396	0.113
+ SDSS4 (linear)	11264.9/12.2	1.1/-0.8	0.955	1.12×10^{-5}	0.0347	0.0666
SDSS1 + WMAP1	1452.5/23.6	0.9/2.2	0.959	8.36×10^{-7}	0.147	0.397
SDSS1 + WMAP3	11278.1/24.3	0.9/2.2	0.943	6.18×10^{-7}	0.131	0.222
SDSS4 + WMAP1	1453.7/24.3	1.6/4.1	0.950	24.0×10^{-7}	0.0850	0.223
SDSS4 + WMAP3	11276.9/24.2	0.4/2.4	0.945	9.76×10^{-7}	0.0725	0.0567
Ly- α + WMAP1	1454.1/24.9	2.5/3.3	0.973	1.05×10^{-9}	1.49	0.521
Ly- α + WMAP3	11279.9/26.9	2.5/3.8	0.959	0.612×10^{-9}	1.49	0.331

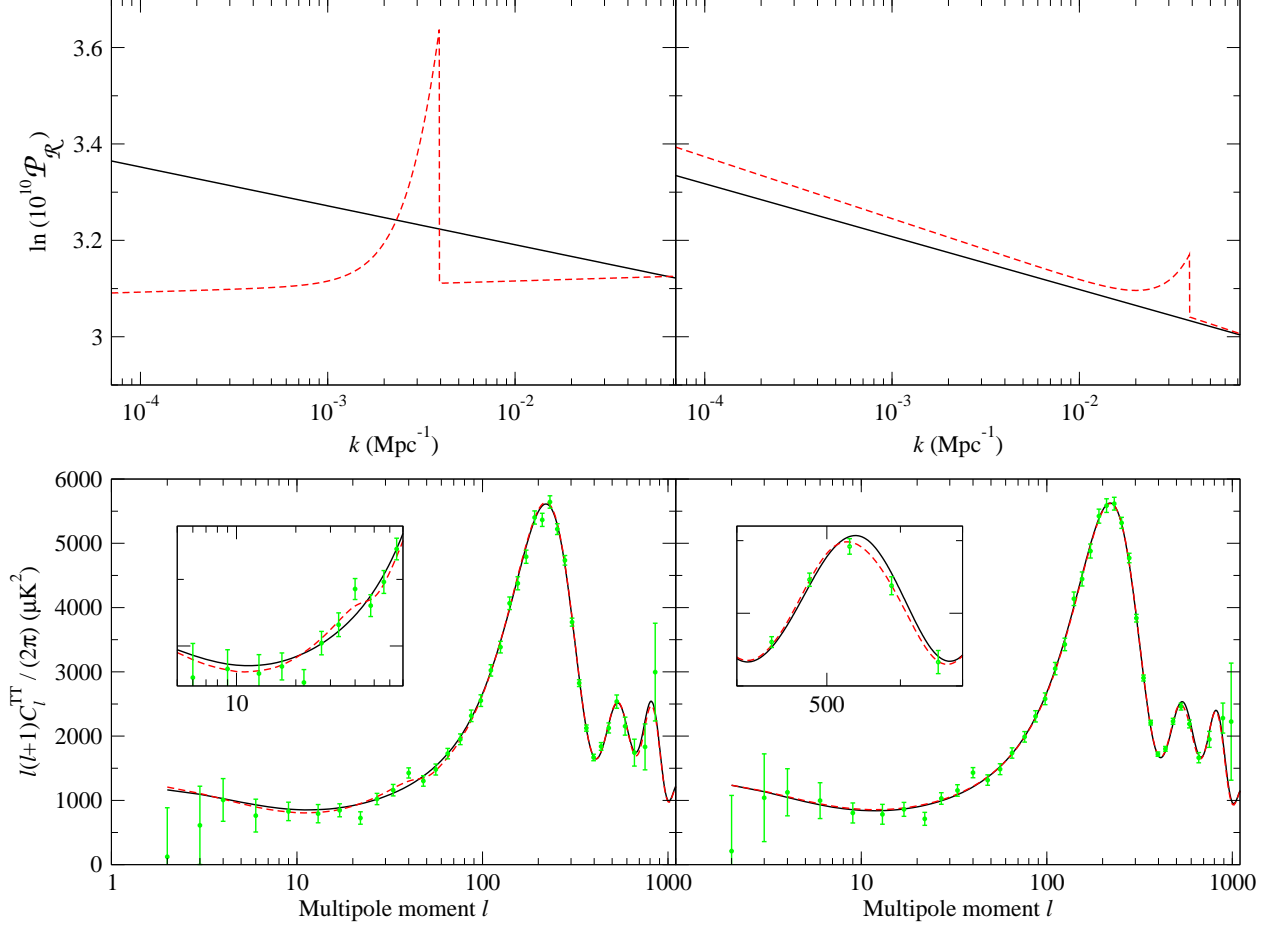


Figure 1: The best fit primordial power spectra (upper) and C_ℓ^{TT} spectra (lower) for the power-law ΛCDM model (solid, black) and the k_c^3 model (dashed, red) using the WMAP1 (left) and WMAP3 (right) data (dotted, green). The scales of the wave numbers k (Mpc^{-1}) are shifted to match those of the multipole moment ℓ .

oscillations to some extent, it is not surprising that the k^3 model can offer an alternative physical explanation for the improved fits found in Refs. [23, 24, 25, 26].

As for WMAP3, Table 1 and Fig. 1 show that the best fit k^3 peak appears around 0.04 Mpc^{-1} , close to the second peak ($\ell \sim 540$) of the C_ℓ^{TT} spectrum (see the right panels of Fig. 1). This can be understood due to the failure of the best fit ΛCDM model to match the data within 1σ in this region. Due to improved sensitivity of WMAP3 to these higher multipoles, the “glitch” at $\ell \sim 540$ is statistically more significant to WMAP3 than to WMAP1, where the $\ell \sim 10 - 50$ glitch took precedence. This explains why the best fit power spectra of WMAP1 and WMAP3 are very different (see Fig. 1). We emphasize that these results are consistent with each other. One could have the k^3 peak appear at 0.004 Mpc^{-1} for WMAP3, but the resultant $\Delta\chi^2$ is smaller ($\Delta\chi^2 = 2.0$); similarly, one could adjust the k^3 component to fit the high multipoles of WMAP1, but the $\Delta\chi^2 = 1.2$ is smaller than that of fitting the low multipoles. (Of course, it is possible for a single data set to favor, to some extent, the simultaneous appearance of the k^3 feature at different scales; one of the objective of this

paper is to constrain such an effect, which will be given in Section 5.4.) Obviously, a more complicated primordial power spectrum could have a better fit. In particular, introducing an additional k^3 peak at 0.004 Mpc^{-1} while keeping the k^3 peak at 0.04 Mpc^{-1} fits better than either peak by itself. References [25, 26] make a similar observation; by changing the location and amplitude of the oscillations, their model is able to fit different ranges of multipoles. Unlike the oscillations which affect all multipoles beyond the second peak of the CMB power spectrum, the effect of the k^3 component for WMAP3 in the best fit model is localized at the second peak.

Figure 2 shows the distributions of the parameters for the power-law Λ CDM model (black) and the k_c^3 model (red) using the WMAP3 data. Solid (Λ CDM) and dashed (k_c^3) lines are marginalized probabilities, and dotted (Λ CDM) and dot-dashed (k_c^3) lines are mean likelihoods of samples; for Gaussian distributions, they should be the same. The mean likelihoods indicate whether the parameters are really being constrained, or affected by the priors and the volume of samples; they also show how good a fit one can expect [59]. There are four Markov chains for the model, and they satisfy the Gelman and Rubin convergence test $R - 1 < 0.03$. The Gelman and Rubin “variance of chain means” / “mean of chain variances” convergence test generally demands that $R - 1 < 0.1$ for each parameter; for example, the WMAP collaboration demands that $R - 1 < 0.1$ [5]. However, smaller numbers usually indicate better convergence.⁵

One can see from Fig. 2 that introducing the k^3 component does not have significant statistical influence on the standard parameters. Nevertheless, there are inconsistencies between the marginalized probabilities and the mean likelihoods of samples at the higher ends of $\Omega_b h^2$, $\Omega_c h^2$, θ , n_s , and $\ln P_\phi$. These inconsistencies, along with the small bumps of $\ln r_3$ and $\ln k_c$, indicate that there is another local best fit point in the parameter space, i.e. the k_c^3 model, which fits the low multipoles. This can be seen in the corresponding probabilities for WMAP1 (which we do not show): there the smaller bumps seen in the distributions for WMAP3 become the more significant features, and shift the most likely values.

We also notice that the marginalized probabilities of $\ln r_3$ and $\ln k_c$ are far from Gaussian. This is related to the priors of $\ln r_3$ and $\ln k_c$:

$$-25 < \ln r_3(k_0) < 0, \quad (5)$$

$$-8 < \ln k_c [\text{Mpc}^{-1}] < -0.25. \quad (6)$$

To justify these priors, we note that the amplitude ratio $\ln r_3(k_0) = -25$ gives a negligible k^3 component even on small scales, i.e. $r_3(1 \text{ Mpc}^{-1}) \sim 10^{-3}$. On the other hand, if $\ln r_3(k_0) > 0$, then the k^3 component will dominate over the primordial power spectrum and it should have been observed. The prior of $\ln k_c$ is set to cover observable k space: $\ln k [\text{Mpc}^{-1}] = -8$ roughly corresponds to the largest observable scale and $\ln k [\text{Mpc}^{-1}] = -0.25$ is the highest value found to be called by CosmoMC when the CMB data are used. These are not true priors in any rigorous sense. From a phenomenological perspective these models are unbounded from below and any proper Bayesian estimate of parameters is likely to be swamped by the large part of the allowed parameter space that provides effectively no observed deviations

⁵See CosmoMC’s website, <http://www.cosmologist.info/cosmomc>, for further discussions.

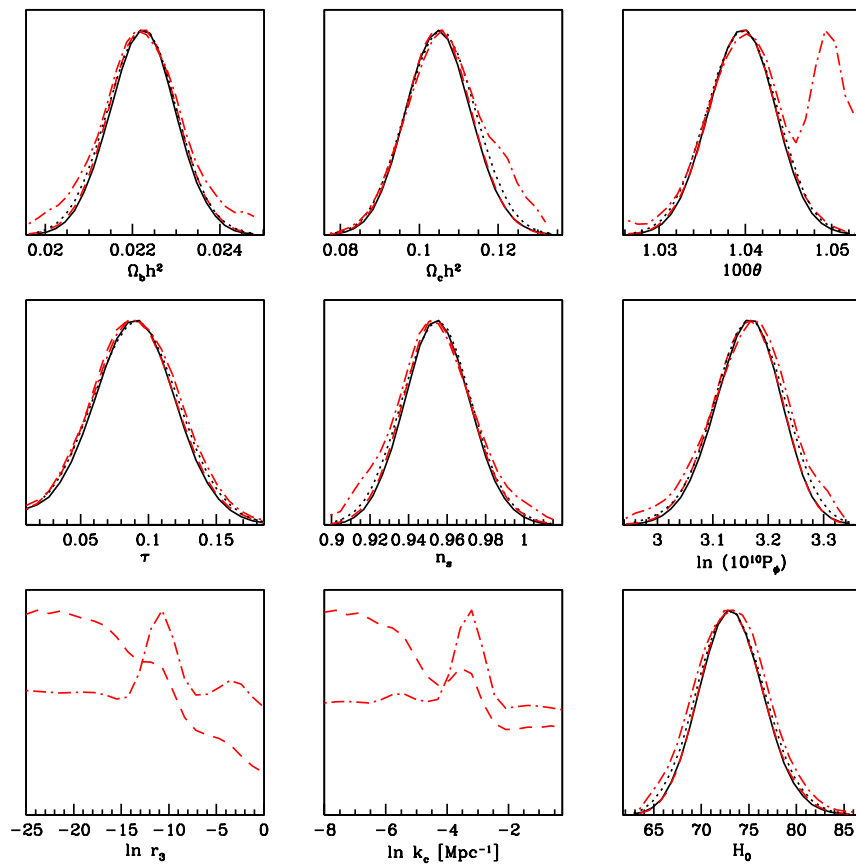


Figure 2: The distributions of the parameters for the power-law Λ CDM model (black) and the k_c^3 model (red) using the WMAP3 data. Solid (Λ CDM) and dashed (k_c^3) lines are marginalized probabilities; dotted (Λ CDM) and dot-dashed (k_c^3) lines are mean likelihoods of samples. ($k_0 = 0.002 \text{ Mpc}^{-1}$.)

from scale invariance. This can be seen in the marginalized probabilities of Fig. 2. However, for understanding to what extent the data allow such deviations these priors permit practical exploration of the allowed parameter space.

The choice of priors still allows for degeneracies. For any value of $\ln r_3$ in the prior, taking the minimum value of $\ln k_c$ makes the k^3 contributions negligible, and vice versa. This fact explains why the higher tails of the $\ln r_3$ and $\ln k_c$ distributions in Fig. 2 do not decay, since the k_c^3 model becomes the power-law Λ CDM model in that region and has a large volume of samples. Similarly, the lower ends of the $\ln r_3$ and $\ln k_c$ distributions have a larger range where the k^3 component is negligible and hence give rise to higher values of marginalized probabilities, as seen in Fig. 2.

Plotting the two-dimensional marginalized surfaces makes the argument clearer. Figure 3 shows the two-dimensional marginalized probabilities (and their 68% and 95% CL contours) and mean likelihoods of samples of $\ln r_3$ and $\ln k_c$ for the k_c^3 model using the WMAP3 alone

(left), and in combination with SDSS4 (linear) and Viel *et al.* Lyman- α data (right). (See Section 5.4 for further discussions.) The waterfall shape surfaces demonstrate that the high $\ln r_3$ and $\ln k_c$ regions are ruled out by the data. The high plateaus are the regions having a negligible k^3 component and a large volume of samples. The peaks in the probabilities and mean likelihoods of samples represent the best fit models. We normalize the marginalized probabilities and mean likelihoods of samples at their maximum points and show them in logarithmic scales, so that one can see how far the plateaus are from the best fit points in terms of $\Delta\chi^2 \sim -2 \ln L$.⁶ As we discussed above, there are two peaks in the mean likelihood of samples, the smaller one corresponding to fitting the glitch at low multipoles.⁷ Since the plateau is near the 1σ confidence level, the projection of the two-dimensional marginalized probabilities shows many contours where the surface crosses 1σ ; see the bottom panels of Fig. 3.

Table 2 lists the best fit models and marginalized values for the power-law Λ CDM model and the k_c^3 model using the WMAP3 data. Due to the points just discussed, the one-dimensional marginalized values do not give a good estimate or reliable upper limits on $\ln r_3$ and $\ln k_c$. (However, we will give constraints on the maximum amplitude ratio in Section 5.4.) Nevertheless, the improvements of fitting the irregularities at the low multipoles ($\ell \sim 10-50$) or the second peak ($\ell \sim 540$) could give an additional contribution as large as 14% to 69% to the nearly scale-invariant spectrum (see Table 1). This observation not only provides evidence for the k_c^3 model but also demonstrates the extent to which the data still leave open the possibility of large deviations from scale invariance in the power spectrum.

Furthermore, Fig. 2 shows that the best fit points can have significant variations from the Λ CDM values, as can be seen from the mean likelihoods of samples. With our choice of priors these points contribute little to the marginalized likelihoods, but it is surprising that adding localized features can move physical parameters such as the angular size of the sound horizon by order “ 1σ .” With future polarization data this should be less of an issue, but the robustness of physical parameters to the physics of inflation could be important for future dark energy studies that rely on CMB-derived physical parameters.

5 Fitting Small Scales

To explore the evidence for the k^3 component on small scales, we now focus on other CMB, LSS, and Lyman- α data. The results are discussed in detail in the following subsections.

5.1 Fitting High- ℓ CMB or LSS Data

Including the CBI and ACBAR data allows us to test for the possible presence of the k^3 component in the high- ℓ regime. The best fit models are listed in Table 1. As can be seen, the best fit power spectra of joint WMAP, CBI, and ACBAR are close to those of fitting

⁶Some of the points at the bottom of the waterfall are zero, so their logarithm will give negative infinities. To solve this problem, we plot $2 \ln(L + \epsilon)$ instead, where we take $\epsilon = 4 \times 10^{-6}$ so that the minimum values are -25 , roughly 5σ from the best fit points.

⁷The peaks are not obvious, since they are plotted on a logarithmic scale.

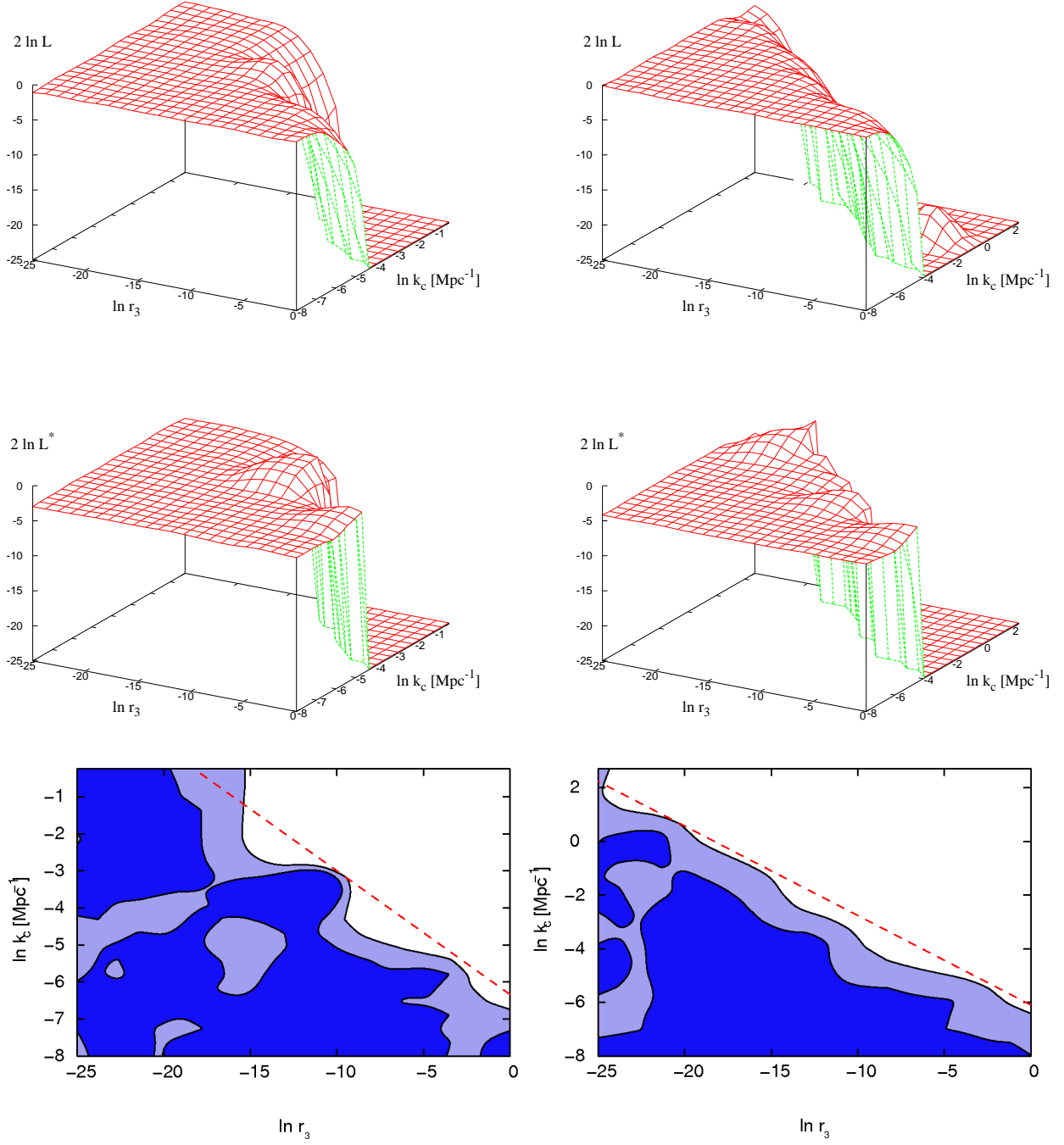


Figure 3: The two-dimensional marginalized probabilities (top; $2 \ln L$), mean likelihoods of samples (middle; $2 \ln L^*$), and marginalized probability contours (bottom; 68% and 95% CL) of $\ln r_3$ and $\ln k_c$ for the k_c^3 model using the WMAP3 alone (left), and in combination with SDSS4 (linear) and Viel *et al.* Lyman- α data (right). The dashed (red) lines in the marginalized probability contours give the best bounds on the amplitude ratio over the observable wave numbers (see Section 5.4). The surface plots have an artificial floor of $2 \ln L = -25$ inserted for plotting purposes (see footnote 6).

Table 2: The best fit power-law Λ CDM model and the k_c^3 model, and their marginalized (mean, 68% CL) values for the WMAP3 data.

Parameter	Λ CDM		k_c^3	
	Best fit	Mean	Best fit	Mean
$10^2\Omega_b h^2$	2.22	$2.22^{+0.07}_{-0.07}$	2.24	$2.22^{+0.07}_{-0.07}$
$\Omega_c h^2$	0.105	$0.105^{+0.008}_{-0.008}$	0.112	$0.105^{+0.008}_{-0.008}$
$10^2\theta$	1.040	$1.040^{+0.004}_{-0.004}$	1.043	$1.040^{+0.004}_{-0.004}$
τ	0.090	$0.090^{+0.029}_{-0.029}$	0.092	$0.089^{+0.030}_{-0.030}$
$n_s(k_0)$	0.952	$0.955^{+0.016}_{-0.016}$	0.944	$0.955^{+0.017}_{-0.017}$
$\ln 10^{10}\mathcal{P}_\phi(k_0)$	3.17	$3.16^{+0.06}_{-0.06}$	3.21	$3.16^{+0.06}_{-0.06}$
$\ln r_3(k_0)$	–	–	–11.0	–15.3 ^a
$\ln k_c$ [Mpc ^{–1}]	–	–	–3.25	–4.81 ^a
h	0.728	$0.732^{+0.032}_{-0.032}$	0.716	$0.733^{+0.032}_{-0.032}$

^aSee Section 5.4 for the constraints.

WMAP alone. This implies that the improvements to the fits come primarily from the WMAP data ($\ell \sim 10 - 50$ or $\ell \sim 540$), and hence the CBI and ACBAR data do not seem to give any additional evidence for a k^3 component. Although there is some excess power in the CBI and ACBAR data at small scales, $\ell > 1000$, this cannot be attributed to the k^3 effect because Silk damping (also known as diffusion damping) kills any sensitivity of the CMB to the primordial power spectrum in this region. Any perturbation to the exponential damping tail seen in the CMB angular power spectrum can only arise from astrophysical effects long after inflation. Thus, no evidence for a k^3 component at large k can be obtained just using CMB data.

We therefore consider the evidence for a k^3 component at large k using LSS data. Table 1 shows that the locations and amplitudes of the k^3 peaks are close to those inferred from the WMAP data alone. We see that adding a k^3 peak at large k ($< 0.15h$ Mpc^{–1} for 2dFGRS and SDSS1 [linear]; $< 0.1h$ Mpc^{–1} for SDSS4 [linear]) fails to improve the fit to the galaxy-galaxy power spectrum.

To further quantify the significance of the WMAP data, we compute a quantity $\chi^{2'}$, defined to be the contribution to the total χ^2 coming from all data except WMAP. These values are shown in Table 1. Since the k^3 peaks at ~ 0.004 Mpc^{–1} (WMAP1) are outside the ranges of the CBI, ACBAR, 2dFGRS, and SDSS (linear) data which we use (see Section 3), these data are not directly sensitive to such a k^3 component. Indirectly, however, they have an effect, since the best fit k_c^3 model of WMAP1 favors a bluer tilt than do the CBI and ACBAR data. This explains why the k^3 peak at low k is somewhat disfavored by these

data: $\Delta\chi^{2'} = -2.5$. On the other hand, for the k^3 peak at $\sim 0.04 \text{ Mpc}^{-1}$ (WMAP3), the high- ℓ CMB and LSS data exhibit no preference, giving $\Delta\chi^{2'}$ of order $O(0.5)$. Thus, although the CMB and LSS data do not give positive evidence, they are still consistent with a k^3 component which introduces a perturbation on the nearly scale-invariant primordial spectrum whose magnitude is 7% to 18%.

5.2 Fitting the Nonlinear Regime

The SDSS data also probe the nonlinear regime, and we include data up to $k/h = 0.2 \text{ Mpc}^{-1}$, as recommended by the SDSS team. As reference models, we consider the power-law ΛCDM model taking into account nonlinear evolution effects; we also fit the k_c^3 model using the nonlinear theory. The total χ^2 's, the χ^2 's of the galaxy-galaxy power spectra, and the best fit k_c^3 models are shown in Table 1. As can be seen from the table, the results of WMAP1 or WMAP3 plus SDSS1 are consistent, and both k_c^3 models fit slightly better than the power-law ΛCDM model.

Figure 4 shows the best fit galaxy-galaxy power spectra of WMAP + SDSS1 for the power-law ΛCDM and k_c^3 models using nonlinear theory (fitting to $k/h = 0.2 \text{ Mpc}^{-1}$). The vertical shifts between the results of WMAP1 and WMAP3 are probably due to the shift of n_s from 0.959 to 0.943. The bumps at $k/h \sim 0.18 \text{ Mpc}^{-1}$ are believed to be the results of the k^3 peaks in the same regime. Therefore, our results show that, except for the low ($k \sim 0.004 \text{ Mpc}^{-1}$) and high ($k \sim 0.04 \text{ Mpc}^{-1}$) multipoles, the k^3 component could also appear in the nonlinear regime ($k \sim 0.14 \text{ Mpc}^{-1}$). However, since it is not theoretically well-understood how a power spectrum with a k^3 component goes nonlinear, further investigation is needed before drawing any firm conclusions.

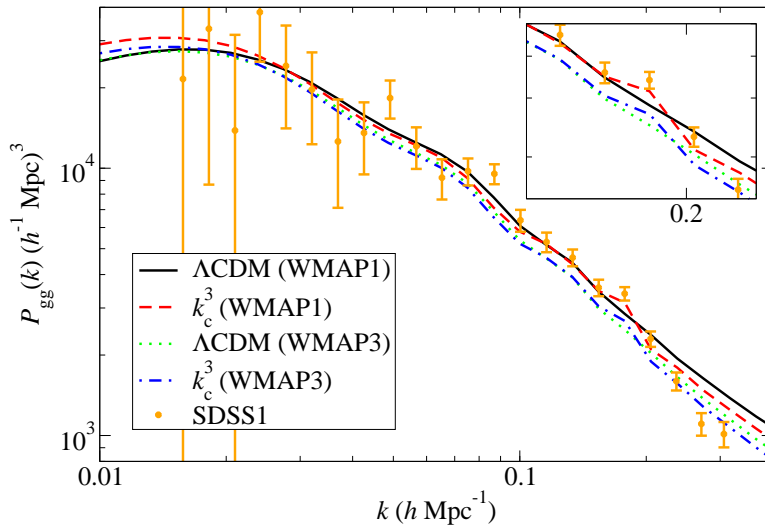


Figure 4: The best fit galaxy-galaxy power spectra of WMAP + SDSS1 for the power-law ΛCDM model and the k_c^3 model (going up to $k/h = 0.2 \text{ Mpc}^{-1}$). The SDSS1 data are also shown.

Table 1 also shows the results of fitting WMAP and SDSS4. The k^3 component can fit the data well ($\Delta\chi^{2'} = 2.4$ for WMAP3 + SDSS4). However, the bumps caused by the

k^3 component are not as obvious as in the SDSS1 samples, so the power spectra of SDSS4 are not shown. The total $\Delta\chi^2$'s are smaller in the case of SDSS4 because the LRG sample favors a lower cutoff, $k \sim 0.08 \text{ Mpc}^{-1}$, where the WMAP data are better fit by a nearly scale-invariant spectrum.

We emphasize that when the nonlinear SDSS data are included, one can still adjust the k^3 component to appear in the WMAP regime. For example, the global best fit model for WMAP3 + SDSS1 has $\Delta\chi^2 = 2.1$ (though $\Delta\chi^{2'} = -0.4$), which is slightly better than for the best fit model where the k^3 component appears in the nonlinear regime ($\Delta\chi^2 = 0.4$ and $\Delta\chi^{2'} = 2.4$).

5.3 Fitting the Lyman- α Data

The Lyman- α forest probes the highest- k regime, and it usually has a large effective redshift ($z > 2$). Therefore, even though it is probing smaller scales, the scales are still in the linear regime because it is looking at early times (smaller scales go nonlinear first).

As mentioned in Section 3, we use two different Lyman- α data sets to test the k^3 component: Viel *et al.* [12, 13, 14] and SDSS Lyman- α [15, 16] data. The lower part of Table 1 lists the best fit k_c^3 models of WMAP + Viel *et al.* Lyman- α . Figure 5 shows the corresponding best fit linear power spectrum at $z = 2.125$ and 2.72 , respectively. The results of WMAP1 and WMAP3 are consistent except for the vertical shifts, which are probably due to the change of the spectral index from 0.973 to 0.959. In this case, the improved fit ($\Delta\chi^{2'} = 3.8$ for WMAP3 + Lyman- α) is due to accounting for a bump at $\sim 0.02 \text{ (km/s)}^{-1}$ in the observed power, which corresponds to a k^3 peak in the primordial power spectrum near $\sim 1.5 \text{ Mpc}^{-1}$. The best fit k_c^3 model for WMAP3 + Viel *et al.* has matter density $\Omega_m = \Omega_b + \Omega_c = 0.27$, so the correspondence between the two different ways of specifying the wave number is given by $1 \text{ (km/s)}^{-1} \sim 97h \text{ Mpc}^{-1}$ for $z = 2.125$ and $1 \text{ (km/s)}^{-1} \sim 104h \text{ Mpc}^{-1}$ for $z = 2.72$ [62]. As in the case of WMAP3 + SDSS1 (nonlinear), the global best fit model of WMAP3 + Viel *et al.* has the k^3 peak appear in the WMAP regime, which gives $\Delta\chi^2 = 5.7$ ($\Delta\chi^{2'} = 0.2$).

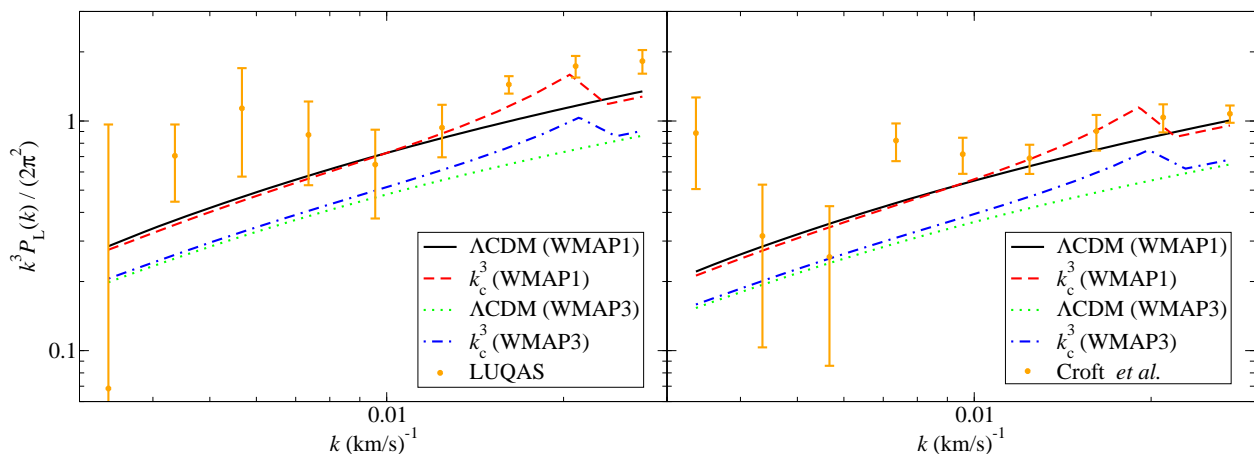


Figure 5: The best fit linear power spectra of WMAP + Viel *et al.* Lyman- α for the power-law Λ CDM model and the k_c^3 model. The LUQAS ($z = 2.125$) and Croft *et al.* ($z = 2.72$) data are also shown.

We also test the k_c^3 model using the SDSS Lyman- α data. It turns out that there is no similar evidence for the k^3 component as in the case of WMAP + Viel *et al.*, i.e. the maximum ratio $r_3(k_c)$ is of order $o(0.01)$, so the k_c^3 model is not distinguishable from the power-law Λ CDM model and hence the $\Delta\chi^2$ is of order $O(0.1)$. At first glance it is a bit surprising that adding two new parameters does not improve the fit substantially. However, the SDSS Lyman- α data are not given in a band-power description of $P_L(k)$; instead, the information is extracted in terms of the amplitude, $k^3 P_L(k, z)/2\pi^2$, its tilt, $n_{\text{eff}} = d \ln P_L(k)/d \ln k$, and the running, $\alpha_{\text{eff}} = dn_{\text{eff}}/d \ln k$, at a pivot redshift $z_p = 3.0$ and a pivot wavenumber $k_p = 0.009 \text{ (km/s)}^{-1}$ [15, 16]. It is not obvious that such a description of the data can accommodate the extra freedom available in the k_c^3 model.

5.4 Constraint on the Amplitude Ratio

In the absence of significant positive evidence for a k^3 distortion, we now consider the experimental limit on the magnitude of the k^3 component in the primordial power spectrum. The right panels of Fig. 3 show the two-dimensional marginalized probabilities (and their 68% and 95% CL contours) and mean likelihood of samples of $\ln r_3$ and $\ln k_c$ for the k_c^3 model using the WMAP3, SDSS1 (linear), and Viel *et al.* Lyman- α data. There are three peaks in the mean likelihood of samples, and they correspond to the local best fits of WMAP (low and high multipoles) and Lyman- α . But only the peak of WMAP (high multipoles) in the marginalized probability can be seen, since it has a large volume of samples.

Again, the waterfall-like surfaces indicate that the high $\ln r_3$ and $\ln k_c$ region is ruled out by the data, but the one-dimensional marginalized constraints on $\ln r_3$ and $\ln k_c$ are meaningless, because of the strong mutual dependence of the two parameters. However, the constraint on $r_3(k_c)$ can be inferred from the two-dimensional marginalized contours. From Eq. (1), the maximum amplitude ratio is

$$r_3(k_c) = r_3(k_0) \left(\frac{k_c}{k_0} \right)^{4-n_s}, \quad (7)$$

so we have

$$\begin{aligned} \ln r_3(k_c) &= \ln r_3(k_0) + (4 - n_s) \ln k_c - (4 - n_s) \ln k_0 \\ &\simeq \ln r_3(k_0) + 3 \ln k_c - 3 \ln k_0, \end{aligned} \quad (8)$$

where we have used the fact that the current best fit model has $n_s \simeq 1$. Therefore, plotting a series of lines with approximately the same $r_3(k_c)$,

$$\ln r_3(k_0) \propto -3 \ln k_c, \quad (9)$$

and finding their intersection with the two-dimensional marginalized contour gives the best bound on the maximum amplitude ratio. From the lower part of Fig. 3 (the dashed, red lines), we find that

$$r_3 < 0.7 \text{ (95\% CL)} \quad \text{for} \quad 1.8 \times 10^{-3} \text{ Mpc}^{-1} < k < 0.3 \text{ Mpc}^{-1} \quad (10)$$

when using WMAP3 alone, and

$$r_3 < 1.5 \text{ (95\% CL)} \quad \text{for} \quad 2.3 \times 10^{-3} \text{ Mpc}^{-1} < k < 8.2 \text{ Mpc}^{-1} \quad (11)$$

when using WMAP3 + SDSS4 (linear) + Viel *et al.* Lyman- α .

It is possible that for a heavy tachyon, the cutoff on its perturbations lies below the smallest currently observable scales. Hence, we also investigate the model without a cutoff, i.e. the k^3 model. From the point of view of the algorithm, this is equivalent to putting the cutoff below the smallest scales in the data or, equivalently, above the largest k value called by CosmoMC. We tested the k^3 model with all the joint data used in the previous sections. All of the results give a negligible amplitude ratio, i.e. $\ln r_3 \rightarrow -25$ (the lower prior), making the model indistinguishable from the power-law Λ CDM model. This gives rise to the following observational constraint on the k^3 model. The upper limit of the magnitude of the k^3 term can be read directly from the bottom-right panel of Fig. 3; taking the largest cutoff value (the upper prior is $k = 15 \text{ Mpc}^{-1}$ when Lyman- α is used) in the contour gives

$$r_3(15 \text{ Mpc}^{-1}) < 11 \text{ (95\% CL)}. \quad (12)$$

6 Theoretical Models

6.1 Hybrid Inflation

In the previous sections we have shown that bumplike features in the power spectra of the CMB and LSS can be explained by the addition of a k^3 contamination of the nearly scale-invariant contribution. We noted in the introduction that preheating at the end of chaotic inflation predicts k^3 components which are too small to be observed on the CMB-LSS scales [49, 50, 51], but recent work has found that observable effects can be generated for some ranges of parameters in hybrid inflation theories [44, 45], which are defined by the potential [63]

$$V(\varphi, \sigma) = \frac{\lambda}{4} (\sigma^2 - v^2)^2 + \frac{m_\varphi^2}{2} \varphi^2 + \frac{g^2}{2} \varphi^2 \sigma^2, \quad (13)$$

where φ is the inflaton and σ is the tachyonic field.

Inflation starts with large values of φ and ends after the field-dependent tachyon mass parameter becomes negative:

$$m_\sigma^2 = -\lambda v^2 + g^2 \varphi^2 < 0. \quad (14)$$

For certain ranges of the parameters v , λ , and g , the fluctuations in σ can become so large that their contribution to the curvature perturbation, at second order in cosmological perturbation theory, exceeds the usual first-order contribution due to the inflaton φ . The growth of fluctuations gets cut off at some number N_* of e-foldings after the onset of the tachyonic instability, when their energy density starts to exceed the false vacuum energy that drives inflation. At this point, inflation ends and there is no further evolution in the curvature perturbation on superhorizon scales. Even if N_* represents a very short amount of time during which the fluctuations can grow in magnitude, they grow exponentially fast, and so it is possible to achieve a large effect.

Without going into all the details, one can still appreciate why it is possible to obtain a spectrum of the form k^3 with a cutoff. In fact, the k^3 spectrum is completely generic for massive fields, i.e. with $m \gg H$, where H is the Hubble scale during inflation. This can be found by solving the Klein-Gordon equation for linearized fluctuations of the fields in de Sitter space; it is straightforward to show that $\langle(\delta\sigma)^2\rangle \sim m^{-1} \int d^3k$ for heavy fields, whereas $\langle(\delta\varphi)^2\rangle \sim H^2 \int d^3k/k^3$ for light ($m \ll H$) fields. However, because of the redshifting of the physical wave number, a k^3 component in the spectrum is usually negligible compared to the scale-invariant contribution. Only if the k^3 component is amplified can it become observable. Thus, the other relevant effect is the amplification of the tachyonic fluctuations by the instability, which causes modes with $k^2 < a^2|m_\sigma^2|$ to grow as $\exp[t\sqrt{|m_\sigma^2| - (k/a)^2}]$. We see that there is naturally a cutoff $k_c = a|m_\sigma|$ on the modes which get amplified. Of course, this scale gets stretched by the Hubble expansion which occurs after inflation. At the present time, the cutoff scale is therefore given by

$$k_c = |m_\sigma| \frac{H_0}{H_i} e^{N_e}, \quad (15)$$

where H_0 and H_i are respectively the Hubble rate today and during inflation, and N_e is the number of e-foldings of inflation since the horizon crossing, $N_e \sim 60$. (In the present analysis, we do not assume that $N_e \sim 60$; rather, we determine N_e according to the actual reheat temperature, assumed to be of the order $\lambda^{1/4}v$ since λv^4 is the false vacuum energy density which drives inflation.) Notice that if $|m_\sigma| = H_i$, k_c/H_0 is just the ratio of scales which crossed the horizon at the beginning and at the end of inflation, as expected. In order to match the bumps in the WMAP data, we need k_c/H_0 to be on the order of 16 or 162. Due to the large factor e^{N_e} in Eq. (15), this is difficult to achieve. However, one should recall that m_σ is field-dependent (Eq. (14)), and it passes through zero shortly before the end of inflation. For some values of parameters, m_σ can still be small at the end of inflation; moreover, N_e can also be relatively small if the reheat temperature is low. It is therefore not obvious whether small enough values of k_c can be achieved to match the phenomenological requirements that were suggested by the previous sections.

To investigate whether the parameters suggested by our fits can correspond to hybrid inflation, we have adapted the code used in Refs. [44, 45], which numerically computed the magnitude r_3 of the k^3 contribution, scanning over a large range of the model's parameters, g , λ , and v . In the left panel of Fig. 6 we plot the values of r_3 (at $k = 1 \text{ Mpc}^{-1}$) versus k_c obtained by scanning over the parameter values $\log_{10} v = -1, -3, -5, -7, -9$, $\log_{10} g^2 > -30$, and $\log_{10} \lambda < 0$. We find no cases where the peak parameters k_c and r_3 are in the range needed for the WMAP glitches at $\ell \sim 10 - 50$ and $\ell \sim 540$ (the diamonds in the figure). The left panel of the figure shows that points having small enough values of k_c all have overly large values of r_3 . However, there are realizations in which k_c is close to the 1 Mpc^{-1} suggested by the Lyman- α data, as well as points where k_c is larger and is effectively removed from the analysis (the k^3 model). Such points are contained in the narrow box shown in the lower right-hand corner of the left panel of Fig. 6.

The promising points in the left panel of Fig. 6 (those falling within the box) correspond to values of the hybrid inflation parameters shown in the right panel of the figure. These are shown as boxes in the g - λ plane, for the values of $\log_{10} v = -1, -3, -5, -7, -9$, along with excluded regions based on the previous analysis of Refs. [44, 45], which demanded that the

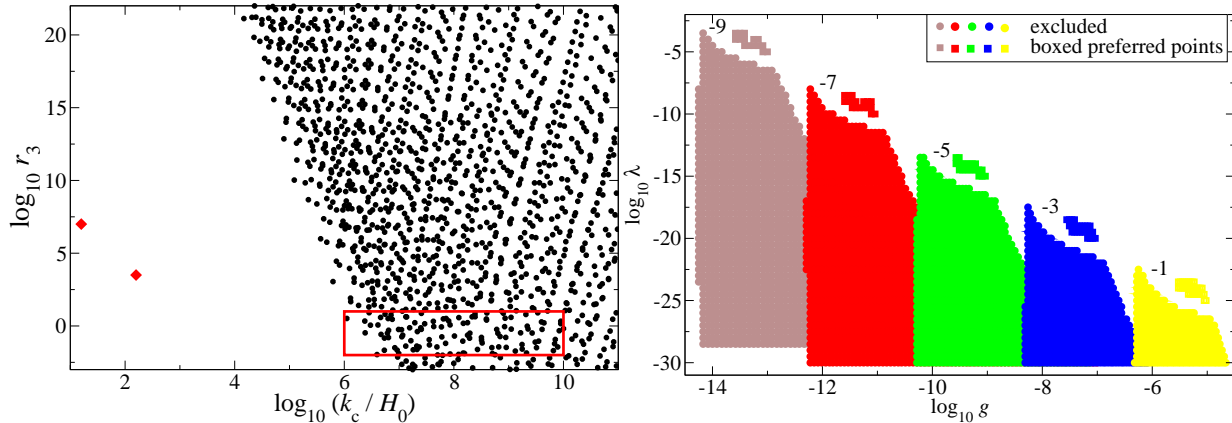


Figure 6: Left: values of r_3 (at $k = 1 \text{ Mpc}^{-1}$) and k_c which are achieved by varying parameters of the hybrid inflation model. The diamonds are the best fit models of WMAP at low and high multipoles; the boxed area is the Lyman- α preferred region $-2 < \log_{10} r_3 < 1$ and $6 < \log_{10}(k_c/H_0) < 10$. Right: preferred points (square) next to excluded regions (circles) for fitting Lyman- α data in the hybrid inflation model. The numbers $(-1, -3, -5, -7, -9)$ indicate the value of $\log_{10} v$ for the respective regions.

k^3 effect not be too large. As expected, the points suggested by our current fits to the data are close to the boundaries of the excluded regions.

6.2 Double D-Term Inflation

We have seen that pure hybrid inflation is able to give a sizeable k^3 component, but with a cutoff k_c larger than the ranges observable in LSS and Lyman- α data. A more complicated but still well-motivated class of models is able to bring k_c into the observable part of the spectrum, as was shown by Ref. [46].⁸ These are double inflation models of the D-term hybrid type [52, 53, 54], based on the superpotential

$$W = \alpha AA_+A_- + \beta BB_+B_-, \quad (16)$$

with six superfields A, A_+, B, B_+ , with charges (g_A, g_B) under two $U(1)$ gauge groups $U(1)_A$ and $U(1)_B$, given by $(0, 0)$ for A, B , $(\pm 1, 0)$ for A_\pm , and $(\pm 1, \pm 1)$ for B_\pm . It leads to a scalar potential of the form

$$V = \frac{g_A^2}{2} \left(\xi_A - \frac{1}{2}|C|^2 \right)^2 + \frac{1}{4}\beta B^2|C|^2 + \frac{g_B^2}{2} \left(\xi_B - \frac{1}{2}|C|^2 \right)^2, \quad (17)$$

plus one-loop corrections (depending on A, B, C), where ξ_i are Fayet-Iliopoulos terms, A and B are proportional to the modulus of the scalar component of the corresponding superfields, and C is the complex scalar component of B_- .

From the form of (17) it can be seen that the field C becomes tachyonic when B rolls down to a critical value. However, in this model, the instability of C need not trigger the end

⁸We thank Julien Lesgourgues for calling our attention to this work.

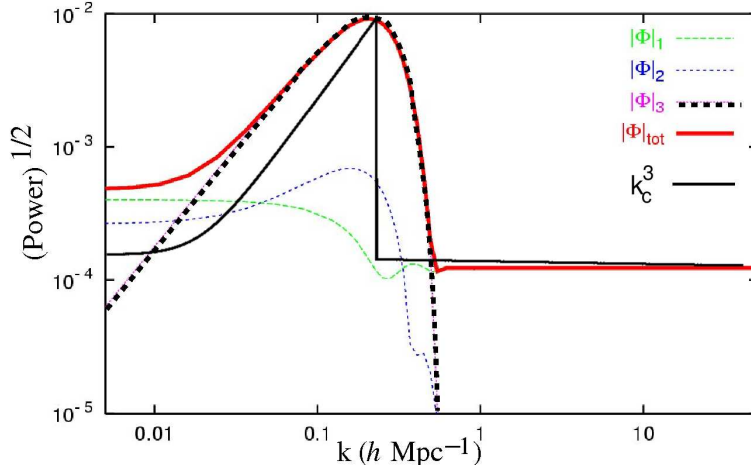


Figure 7: A sample power spectrum from double D-term inflation, adapted from Ref. [46]. The bold dashed line is the k^3 contribution from tachyonic fluctuations. The model parameters were $\sqrt{\xi_A} = 3 \times 10^{-3} M_{\text{Pl}}$, $\sqrt{\xi_B} = 4.2 \times 10^{-3} M_{\text{Pl}}$, $g_A = g_B = 10^{-2}$, and $\beta = 0.5 \times 10^{-3}$. For comparison, a k_c^3 model is also shown, with parameters $r_3(k_0) = 1.3 \times 10^{-3}$ and $k_c = 0.3 h \text{ Mpc}^{-1}$.

of inflation; instead, there can be a second stage via rolling of the field A . The fluctuations due to the tachyonic preheating are found to have a k^3 spectrum, and a sharp cutoff at the scale which crossed the horizon during the phase transition. A k^3 spike is generated, as shown in Fig. 7. In this example, the spike is located at rather high k values, but there is plenty of freedom in the model to move this to arbitrarily lower scales. One merely needs to adjust the duration of the second stage of inflation so that the phase transition occurs sufficiently soon after horizon crossing of modes which are at the present horizon. This model is therefore a good candidate for generating the bumps in the low multipoles which we have investigated in Section 4. We also show a k_c^3 power spectrum in Fig. 7. By appropriate choices of the parameters of the double D-term inflation, the wavenumber and the amplitude of the feature can be adjusted. However, the most closely corresponding spike in the k_c^3 model has a narrower width, so one would have to add another parameter to the k_c^3 ansatz so as to accurately mimic the prediction of the double D-term inflation scenario.

7 k^n Features in the Primordial Power Spectrum

As mentioned in the previous sections, the k_c^3 model is theoretically well motivated, and we take the point of view that it is a good representative of the generic spikelike feature in the primordial power spectrum. To clarify this point, we compare the k_c^3 model to the k_c^n models with nearby values ($n = 1, 2, 4, 5$). Since the evidence from LSS and Lyman- α data is moderate, we focus on the WMAP3 data. Table 3 shows the best fit models for different k^n spike power spectra.

It can be seen from the table that all k_c^n models are consistent: a k^n spike at $k \sim 0.004 \text{ Mpc}^{-1}$ can fit the low-multipole glitches ($\ell \sim 10-50$) and a k^n spike at $k \sim 0.04 \text{ Mpc}^{-1}$

Table 3: The best fit k_c^n models of WMAP3, fitting to the low multipoles ($\ell \sim 10 - 50$, upper) or the second peak ($\ell \sim 540$, lower) of the CMB angular spectrum.

Model	$\Delta\chi^2$	$n_s(k_0)$	k_c (10^{-2} Mpc $^{-1}$)	$r_n(k_c)$
k^1	0.2	0.970	0.434	0.159
k^2	1.2	0.985	0.384	0.446
k^3	2.0	0.969	0.376	0.397
k^4	1.5	0.974	0.382	0.271
k^5	1.9	0.981	0.369	0.797
k^1	5.8	0.944	3.94	0.123
k^2	4.3	0.942	3.82	0.153
k^3	5.4	0.944	3.88	0.139
k^4	4.8	0.946	3.80	0.200
k^5	5.4	0.959	3.79	0.191

can improve the fits of the second peak ($\ell \sim 540$) of the CMB angular spectrum. While all k^n spikes have roughly the same order of improvement ($\Delta\chi^2$), it is interesting that the k^3 model is slightly favored by the data.

We emphasize that the power n is fixed at $n = 3$ in most of the investigation; only in this section so we allow it to change to some nearby values, to show that $n = 3$ is a good representative of the generic spikelike feature.

8 Conclusions

We have examined a class of perturbations to the nearly scale-invariant spectrum, coming from preheating, which is motivated by very general principles of causality. It gives a k^3 component which adds to the usual k^{n_s-1} spectrum, up to some cutoff k_c which is determined by the microphysics of preheating. We did a phenomenological analysis of this kind of distortion to the primordial power spectrum, using the Monte-Carlo Markov-chain algorithm provided by CosmoMC, and found that such a component could improve either the fits to the irregularities of the low multipoles ($\ell \sim 10 - 50$) or the second peak ($\ell \sim 540$) of the CMB spectrum, giving $\Delta\chi^2 = 3.6$ or 1.2 at the low multipoles and $\Delta\chi^2 = 2.0$ or 5.4 at the second peak, using the WMAP1 or WMAP3 data, respectively. Moreover, the amplitude of the k^3 contribution was found to be as large as 0.69 or 0.14 of the k^{n_s-1} part when fitting the low multipoles or the second peak, respectively. These results provide an intriguing suggestion for such a k^3 component, but more generally they indicate that the WMAP data are consistent with sizable deviations from a nearly scale-invariant spectrum.

We also studied the CBI and ACBAR data to investigate whether the k^3 component could explain excess power in the high multipoles seen by those experiments. Our results show that the CBI and ACBAR data are consistent with a k^3 component at the low multipoles or the second peak, but they do not give evidence for a k^3 component at the high multipoles; in retrospect this had to be the case, due to Silk damping. However, this limitation does not apply to LSS data, i.e. 2dFGRS and SDSS, which explore a similar range of k space as CBI and ACBAR. Again, the LSS data are consistent with the results from WMAP, but there is no evidence for the k_c^3 model at $k/h < 0.15 \text{ Mpc}^{-1}$ (0.1 Mpc^{-1} for SDSS4).

We also tested the k_c^3 model in the nonlinear regime of the galaxy-galaxy spectrum, $k/h > 0.15 \text{ Mpc}^{-1}$ (0.1 Mpc^{-1} for SDSS4). We found that the k^3 component can tune the shape of the SDSS galaxy-galaxy power spectrum, giving an improvement of $\Delta\chi^2 = 0.9$ ($\Delta\chi^{2'} = 2.2$) for SDSS1; SDSS4 favors a lower cutoff, $k \sim 0.8 \text{ Mpc}^{-1}$, which gives $\Delta\chi^2 = 0.4$ ($\Delta\chi^{2'} = 2.4$). However, we feel that the implementation of nonlinear evolution in the likelihood code for SDSS has not yet been tested thoroughly in conjunction with a nonstandard spectrum such as the one we are using, so we reserve judgment as to these particular results. They should be taken as motivation for a more detailed study of the nonlinear regime.

A further handle on the power spectrum at high k is provided by the Lyman- α forest data. We found that the Viel *et al.* data allow a large amplitude ratio (0.33), with an improvement of $\chi^2 = 2.5$ ($\Delta\chi^{2'} = 3.8$). The SDSS Lyman- α data, however, do not give similar evidence in the same regime.

In brief, the CMB, LSS, and Lyman- α data are consistent with a nearly scale-invariant spectral index plus a k^3 component. We further showed that the k^3 spike is a good representative of the generic spikelike feature in the primordial power spectrum by comparing different k_c^n models. By adjusting both the location and the amplitude of the k^3 component, one can of course always find better fits. We emphasize that due to the addition of two free parameters, the evidence for the k^3 component is not compelling. However, our results show that the k_c^3 contamination is not ruled out by the data, even when its amplitude is surprisingly large. We have determined constraints on the magnitude of this extra component, finding an upper limit of $r_3 < 1.5$ (95% CL) on the amplitude ratio, over the range of wave numbers $2.3 \times 10^{-3} \text{ Mpc}^{-1} < k < 8.2 \text{ Mpc}^{-1}$.

We have also explored in some detail the parameter space of the hybrid inflation model, which was found to give an observably large k^3 component for some ranges of the model's parameters. The model is able to match the observations in the cases where the benefit of the k^3 component is less rigorously shown, namely in the highest- k regions of the spectrum. For the features at lower k , the double D-term inflation model discussed in Section 6.2 appears to be ideally suited for generating spikes at the large scales we have investigated here.

Acknowledgements

We thank Gilbert Holder for his collaboration in the initial stages of this work, Neil Barnaby for helpful discussions, and Antony Lewis, Anže Slosar, and Patrick McDonald for help with CosmoMC and its SDSS Lyman- α patch. We are grateful to Julien Lesgourgues for constructive criticism of the manuscript. Loison Hoi is supported by the Dow-Hickson Fellowship in Physics at McGill University. We are also supported by NSERC of Canada and FQRNT of

Québec.

A Relation of the k^3 Spectrum to the Causality Constraint

Due to changes of notation over the years, readers of the original causality argument due to Abbott and Traschen [43] may not immediately perceive that their result implies the k^3 spectrum for causal perturbations. In this appendix we clarify the relation. Reference [43] assumes that $\delta\rho(\mathbf{x})/\rho = \sum_a c_a F_a(\mathbf{x} - \mathbf{x}_a)$, where for convenience c_a is a random variable which obeys $\langle c_a c_b \rangle = c^2 \delta_{ab}$. The correlation function in position space is

$$\left\langle \frac{\delta\rho(\mathbf{x})}{\rho} \frac{\delta\rho(\mathbf{y})}{\rho} \right\rangle = c^2 \sum_a F_a(\mathbf{x} - \mathbf{x}_a) F_a(\mathbf{y} - \mathbf{x}_a). \quad (18)$$

In Fourier space,

$$\left\langle \frac{\delta\rho_{\mathbf{k}}^*}{\rho} \frac{\delta\rho_{\mathbf{k}'}}{\rho} \right\rangle = c^2 \sum_a e^{i(\mathbf{k}-\mathbf{k}') \cdot \mathbf{x}_a} k^2 k'^2, \quad (19)$$

where we assumed that each F_a has Fourier transform $F_{a\mathbf{k}} \sim |\mathbf{k}|^2 = k^2$, which is the essential restriction due to causality. If there are enough random centers \mathbf{x}_a , then the sum will approximately give a delta function,

$$\left\langle \frac{\delta\rho_{\mathbf{k}}^*}{\rho} \frac{\delta\rho_{\mathbf{k}'}}{\rho} \right\rangle \simeq c^2 \left(\frac{2\pi}{L} \right)^3 k^2 k'^2 \delta_{\mathbf{k}\mathbf{k}'}, \quad (20)$$

where L is a box size. Therefore, one has

$$\left\langle \left| \frac{\delta\rho_{\mathbf{k}}}{\rho} \right|^2 \right\rangle \simeq c^2 \left(\frac{2\pi}{L} \right)^3 k^4. \quad (21)$$

The k^4 behavior is potentially confusing, but we will now show that this translates into k^3 behavior for the power spectrum of the curvature perturbation \mathcal{R} .

The relation between $\mathcal{R}_{\mathbf{k}}$ and $\delta\rho_{\mathbf{k}}/\rho$ is [62]

$$\frac{\delta\rho_{\mathbf{k}}}{\rho} = \frac{2}{5} \left(\frac{k}{aH} \right)^2 \frac{D_1(\Omega_m)}{\Omega_m} T(k, \Omega_{m0}) \mathcal{R}_{\mathbf{k}}, \quad (22)$$

where $D_1(\Omega_m)/\Omega_m$ is the growth factor for the matter perturbation and $T(k, \Omega_{m0})$ is the transfer function. Since the growth factor does not have k dependence and the causality argument applies to the limit $k \rightarrow 0$ where $T(k)$ is roughly a constant,

$$\left\langle \left| \frac{\delta\rho_{\mathbf{k}}}{\rho} \right|^2 \right\rangle \sim k^4 \langle |\mathcal{R}_{\mathbf{k}}|^2 \rangle. \quad (23)$$

On the other hand, the power spectrum is defined through

$$\mathcal{P}_{\mathcal{R}}(k) \equiv \left(\frac{L}{2\pi} \right)^3 4\pi k^3 \langle |\mathcal{R}_{\mathbf{k}}|^2 \rangle. \quad (24)$$

Equations (23) and (24) imply that

$$\left\langle \left| \frac{\delta\rho_{\mathbf{k}}}{\rho} \right|^2 \right\rangle \sim \left(\frac{2\pi}{L} \right)^3 \frac{k}{4\pi} \mathcal{P}_{\mathcal{R}}(k). \quad (25)$$

Making a comparison with Eq. (21), we see that

$$\mathcal{P}_{\mathcal{R}}(k) \sim k^3 \quad (26)$$

if $\delta\rho$ has the assumed behavior.

The typical onset value for $T(k)$ to decrease is of order 0.01 Mpc^{-1} . Therefore, if the causality constraint is going to give a k^3 spectrum, then the k^3 component appears only at $k < 0.01 \text{ Mpc}^{-1}$, otherwise the causality constraint will give a power greater than 3. Of course, the decrease of the k^3 component could be more complicated than a sharp cutoff.

References

- [1] A. H. Guth, “Inflationary Universe: A Possible Solution to the Horizon and Flatness Problems,” *Phys. Rev.* **D 23**, 347 (1981).
- [2] A. R. Liddle, “An Introduction to Cosmological Inflation,” in “1998 Summer School in High Energy Physics and Cosmology,” 260, A. Masiero, G. Senjanovic, and A. Smirnov (editors), World Scientific, Singapore (1999) [arXiv:astro-ph/9901124].
- [3] R. H. Brandenberger, “Inflationary Cosmology: Progress and Problems,” in “Large Scale Structure Formation,” 169, R. Mansouri and R. Brandenberger (editors), Kluwer Academic Publishers, the Netherlands (2000) [arXiv:hep-ph/9910410].
- [4] D. N. Spergel *et al.*, “First Year Wilkinson Microwave Anisotropy Probe (WMAP) Observations: Determination of Cosmological Parameters,” *Astrophys. J. Suppl.* **148**, 175 (2003) [arXiv:astro-ph/0302209].
- [5] D. N. Spergel *et al.*, “Wilkinson Microwave Anisotropy Probe (WMAP) Three Year Results: Implications for Cosmology,” *Astrophys. J. Suppl.* **170**, 377 (2007) [arXiv:astro-ph/0603449].
- [6] A. C. S. Readhead *et al.*, “Extended Mosaic Observations with the Cosmic Background Imager,” *Astrophys. J.* **609**, 498 (2004) [arXiv:astro-ph/0402359].
- [7] C. L. Kuo *et al.*, “High Resolution Observations of the CMB Power Spectrum with ACBAR,” *Astrophys. J.* **600**, 32 (2004) [arXiv:astro-ph/0212289].
- [8] W. J. Percival *et al.*, “Parameter Constraints for Flat Cosmologies from CMB and 2dFGRS Power Spectra,” *Mon. Not. Roy. Astron. Soc.* **337**, 1068 (2002) [arXiv:astro-ph/0206256].
- [9] S. Cole *et al.*, “The 2dF Galaxy Redshift Survey: Power-Spectrum Analysis of the Final Dataset and Cosmological Implications,” *Mon. Not. Roy. Astron. Soc.* **362**, 505 (2005) [arXiv:astro-ph/0501174].

- [10] M. Tegmark *et al.*, “Cosmological Parameters from SDSS and WMAP,” *Phys. Rev. D* **69**, 103501 (2004) [arXiv:astro-ph/0310723].
- [11] M. Tegmark *et al.*, “Cosmological Constraints from the SDSS Luminous Red Galaxies,” *Phys. Rev. D* **74**, 123507 (2006) [arXiv:astro-ph/0608632].
- [12] M. Viel, M. G. Haehnelt, and V. Springel, “Inferring the Dark Matter Power Spectrum from the Lyman- α Forest in High-Resolution QSO Absorption Spectra,” *Mon. Not. Roy. Astron. Soc.* **354**, 684 (2004) [arXiv:astro-ph/0404600].
- [13] T. S. Kim, M. Viel, M. G. Haehnelt, R. F. Carswell, and S. Cristiani, “The Power Spectrum of the Flux Distribution in the Lyman-Alpha Forest of a Large Sample of UVES QSO Absorption Spectra (LUQAS),” *Mon. Not. Roy. Astron. Soc.* **347**, 355 (2004) [arXiv:astro-ph/0308103].
- [14] R. A. C. Croft *et al.*, “Towards a Precise Measurement of Matter Clustering: Lyman-Alpha Forest Data at Redshifts 2-4,” *Astrophys. J.* **581**, 20 (2002) [arXiv:astro-ph/0012324].
- [15] P. McDonald *et al.*, “The Lyman-alpha Forest Power Spectrum from the Sloan Digital Sky Survey,” *Astrophys. J. Suppl.* **163**, 80 (2006) [arXiv:astro-ph/0405013].
- [16] P. McDonald *et al.*, “The Linear Theory Power Spectrum from the Lyman- α Forest in the Sloan Digital Sky Survey,” *Astrophys. J.* **635**, 761 (2005) [arXiv:astro-ph/0407377].
- [17] H. V. Peiris *et al.*, “First Year Wilkinson Microwave Anisotropy Probe (WMAP) Observations: Implications for Inflation,” *Astrophys. J. Suppl.* **148**, 213 (2003) [arXiv:astro-ph/0302225].
- [18] J. M. Cline and L. Hoi, “Inflationary Potential Reconstruction for a WMAP Running Power Spectrum,” *JCAP* **0606**, 007 (2006) [arXiv:astro-ph/0603403].
- [19] A. A. Starobinsky, “Spectrum of Adiabatic Perturbations in the Universe when There Are Singularities in the Inflation Potential,” *JETP Lett.* **55**, 489 (1992) [*Pisma Zh. Eksp. Teor. Fiz.* **55**, 477 (1992)].
- [20] J. A. Adams, B. Cresswell, and R. Easther, “Inflationary Perturbations from a Potential with a Step,” *Phys. Rev. D* **64**, 123514 (2001) [arXiv:astro-ph/0102236].
- [21] J. O. Gong, “Breaking Scale Invariance from a Singular Inflaton Potential,” *JCAP* **0507**, 015 (2005) [arXiv:astro-ph/0504383].
- [22] M. Kawasaki, T. Takayama, M. Yamaguchi, and J. Yokoyama, “Power Spectrum of the Density Perturbations from Smooth Hybrid New Inflation Model,” *Phys. Rev. D* **74**, 043525 (2006) [arXiv:hep-ph/0605271].
- [23] A. Shafieloo and T. Souradeep, “Primordial Power Spectrum from WMAP,” *Phys. Rev. D* **70**, 043523 (2004) [arXiv:astro-ph/0312174].

- [24] A. Shafieloo, T. Souradeep, P. Manimaran, P. K. Panigrahi, and R. Rangarajan, “Features in the Primordial Spectrum from WMAP: A Wavelet Analysis,” *Phys. Rev. D* **75**, 123502 (2007) [arXiv:astro-ph/0611352].
- [25] L. Covi, J. Hamann, A. Melchiorri, A. Slosar, and I. Sorbera, “Inflation and WMAP Three Year Data: Features Have a Future!” *Phys. Rev. D* **74**, 083509 (2006) [arXiv:astro-ph/0606452].
- [26] J. Hamann, L. Covi, A. Melchiorri, and A. Slosar, “New Constraints on Oscillations in the Primordial Spectrum of Inflationary Perturbations,” *Phys. Rev. D* **76**, 023503 (2007) [arXiv:astro-ph/0701380].
- [27] D. Tocchini-Valentini, M. Douspis, and J. Silk, “Are There Features in the Primordial Power Spectrum?” *Mon. Not. Roy. Astron. Soc.* **359**, 31 (2005) [arXiv:astro-ph/0402583].
- [28] P. Hunt and S. Sarkar, “Multiple Inflation and the WMAP ‘Glitches’” *Phys. Rev. D* **70**, 103518 (2004) [arXiv:astro-ph/0408138].
- [29] P. Hunt and S. Sarkar, “Multiple Inflation and the WMAP ‘Glitches’ II. Data Analysis and Cosmological Parameter Extraction,” *Phys. Rev. D* **76**, 123504 (2007) [arXiv:0706.2443 [astro-ph]].
- [30] A. Shafieloo and T. Souradeep, “Estimation of Primordial Spectrum with Post-WMAP 3 Year Data,” *Phys. Rev. D* **78**, 023511 (2008) [arXiv:0709.1944 [astro-ph]].
- [31] M. Joy, V. Sahni, and A. A. Starobinsky, “A New Universal Local Feature in the Inflationary Perturbation Spectrum,” *Phys. Rev. D* **77**, 023514 (2008) [arXiv:0711.1585 [astro-ph]].
- [32] L. Verde and H. V. Peiris, “On Minimally-Parametric Primordial Power Spectrum Reconstruction and the Evidence for a Red Tilt,” *JCAP* **0807**, 009 (2008) [arXiv:0802.1219 [astro-ph]].
- [33] C. Pahud, M. Kamionkowski and A. R. Liddle, “Oscillations in the inflaton potential?” *Phys. Rev. D* **79**, 083503 (2009) [arXiv:0807.0322 [astro-ph]].
- [34] M. Joy, A. Shafieloo, V. Sahni, and A. A. Starobinsky, “Is a Step in the Primordial Spectral Index Favored by CMB Data ?,” *JCAP* **0906**, 028 (2009) [arXiv:0807.3334 [astro-ph]].
- [35] A. Shafieloo and T. Souradeep, “Assumptions of the Primordial Spectrum and Cosmological Parameter Estimation,” arXiv:0901.0716 [astro-ph.CO].
- [36] P. Paykari and A. H. Jaffe, “Optimal Binning of the Primordial Power Spectrum,” arXiv:0902.4399 [astro-ph.CO].
- [37] G. Nicholson and C. R. Contaldi, “Reconstruction of the Primordial Power Spectrum using Temperature and Polarisation Data from Multiple Experiments,” *JCAP* **0907**, 011 (2009) [arXiv:0903.1106 [astro-ph.CO]].

- [38] M. J. Mortonson, C. Dvorkin, H. V. Peiris, and W. Hu, “CMB polarization features from inflation versus reionization,” *Phys. Rev. D* **79**, 103519 (2009) [arXiv:0903.4920 [astro-ph.CO]].
- [39] D. Parkinson, P. Mukherjee, and A. R. Liddle, “A Bayesian Model Selection Analysis of WMAP3,” *Phys. Rev. D* **73**, 123523 (2006) [arXiv:astro-ph/0605003].
- [40] C. Pahud, A. R. Liddle, P. Mukherjee, and D. Parkinson, “Model Selection Forecasts for the Spectral Index from the Planck Satellite,” *Phys. Rev. D* **73**, 123524 (2006) [arXiv:astro-ph/0605004].
- [41] A. R. Liddle, P. Mukherjee, and D. Parkinson, “Cosmological Model Selection,” *Astron. & Geophys.* **47**, 4.30 (2006) [arXiv:astro-ph/0608184].
- [42] A. R. Liddle, “Information Criteria for Astrophysical Model Selection,” *Mon. Not. Roy. Astron. Soc. Lett.* **377**, L74 (2007) [arXiv:astro-ph/0701113].
- [43] L. F. Abbott and J. H. Traschen, “Causality Constraints on Cosmological Perturbations,” presented at “International Conference on Singular Behaviour and Nonlinear Dynamics, Vol. 2, Singular Behavior and Nonlinear Dynamics,” Samos, Greece (1988), S. Pnevmatikos, T. Bountis, and S. Pnevmatikos (editors), World Scientific, Singapore (1989).
- [44] N. Barnaby and J. M. Cline, “Nongaussian and Nonscale-Invariant Perturbations from Tachyonic Preheating in Hybrid Inflation,” *Phys. Rev. D* **73**, 106012 (2006) [arXiv:astro-ph/0601481].
- [45] N. Barnaby and J. M. Cline, “Nongaussianity from Tachyonic Preheating in Hybrid Inflation,” *Phys. Rev. D* **75**, 086004 (2007) [arXiv:astro-ph/0611750].
- [46] J. Lesgourgues, “Features in the Primordial Power Spectrum of Double D-Term Inflation,” *Nucl. Phys. B* **582**, 593 (2000) [arXiv:hep-ph/9911447].
- [47] J. H. Traschen, “Constraints on Stress Energy Perturbations in General Relativity,” *Phys. Rev. D* **31**, 283 (1985);
- [48] J. H. Traschen, “Causal Cosmological Perturbations and Implications for the Sachs-Wolfe Effect,” *Phys. Rev. D* **29**, 1563 (1984).
- [49] A. R. Liddle, D. H. Lyth, K. A. Malik, and D. Wands, “Super-Horizon Perturbations and Preheating,” *Phys. Rev. D* **61**, 103509 (2000) [arXiv:hep-ph/9912473].
- [50] F. Finelli and S. Khlebnikov, “Metric Perturbations at Reheating: The Use of Spherical Symmetry,” *Phys. Rev. D* **65**, 043505 (2002) [arXiv:hep-ph/0107143].
- [51] T. Suyama, T. Tanaka, B. Bassett, and H. Kudoh, “Are Black Holes Over-Produced During Preheating?” *Phys. Rev. D* **71**, 063507 (2005) [arXiv:hep-ph/0410247].
- [52] M. Sakellariadou and N. Tetradis, “Spectrum of Cosmological Perturbations from Multiple-Stage Inflation,” arXiv:hep-ph/9806461.

- [53] J. Lesgourgues, “Double D-Term Inflation,” *Phys. Lett. B* **452**, 15 (1999) [arXiv:hep-ph/9811255].
- [54] T. Kanazawa, M. Kawasaki, N. Sugiyama, and T. Yanagida, “Double Inflation in Supergravity and the Large Scale Structure,” *Phys. Rev. D* **61**, 023517 (2000) [arXiv:hep-ph/9908350].
- [55] K. Enqvist and A. Vaihkonen, “Non-Gaussian Perturbations in Hybrid Inflation,” *JCAP* **0409**, 006 (2004) [arXiv:hep-ph/0405103].
- [56] K. Enqvist, A. Jokinen, A. Mazumdar, T. Multamaki, and A. Vaihkonen, “Non-Gaussianity from Preheating,” *Phys. Rev. Lett.* **94**, 161301 (2005) [arXiv:astro-ph/0411394].
- [57] K. Enqvist, A. Jokinen, A. Mazumdar, T. Multamaki, and A. Vaihkonen, “Non-Gaussianity from Instant and Tachyonic Preheating,” *JCAP* **0503**, 010 (2005) [arXiv:hep-ph/0501076].
- [58] K. Enqvist, A. Jokinen, A. Mazumdar, T. Multamaki, and A. Vaihkonen, “Cosmological Constraints on String Scale and Coupling Arising from Tachyonic Instability,” *JHEP* **0508**, 084 (2005) [arXiv:hep-th/0502185].
- [59] A. Lewis and S. Bridle, “Cosmological Parameters from CMB and Other Data: A Monte-Carlo Approach,” *Phys. Rev. D* **66**, 103511 (2002) [arXiv:astro-ph/0205436].
- [60] L. Hoi and G. P. Holder, “The Offset Lognormal Matrix for CBI,” <http://www.physics.mcgill.ca/~hoiloison/cbi> (2006).
- [61] L. Hoi, “Inflationary Spectral Indices and Potential Reconstruction,” M.Sc. thesis, McGill University (2006).
- [62] A. R. Liddle and D. H. Lyth, “Cosmological Inflation and Large-Scale Structure,” Cambridge University Press, Cambridge (2000).
- [63] A. D. Linde, “Hybrid Inflation,” *Phys. Rev. D* **49**, 748 (1994) [arXiv:astro-ph/9307002].